Nitrogen Mustard Induced Protein Influx in Nucleus and Metabolism Change and p97 Mediated the Repair

Jin Cheng
the Third Military Medical University (Army Medical University)
Wenpei Yu
the Third Military Medical University (Army Medical University)
Haoyin Liu
the Third Military Medical University (Army Medical University)
Xunhu Dong
the Third Military Medical University (Army Medical University)
Yan Sai
the Third Military Medical University (Army Medical University)
Feng Ye
the Third Military Medical University (Army Medical University)
Guorong Dan
the Third Military Medical University (Army Medical University)
Mingliang Chen
the Third Military Medical University (Army Medical University)
Yuanpeng Zhao
the Third Military Medical University (Army Medical University)
Xi Zhang
the Third Military Medical University (Army Medical University)
Zhongmin Zou (zmzou@tmmu.edu.cn)
the Third Military Medical University (Army Medical University)

Research Article

Keywords: Proteome, DNA-protein crosslink, nitrogen mustard, nucleus, p97

Posted Date: January 10th, 2023

DOI: https://doi.org/10.21203/rs.3.rs-2448806/v1

Abstract

Nitrogen mustard (NM) can alkylate nucleophilic proteins and DNA, causing severe cell damage. However, there are no reports on NM-induced proteomics dynamic changes. In this study, nuclear and cytoplasmic proteins of 16HBE cell were separated and the components and amounts were detected and analyzed. The amount of DNA protein cross-linking (DPC) and the function of p97 were also explored. One-hour-NM-exposure caused a tremendous number of proteins entered into the nucleus and DPC formation. As repair progressed, proteins exited. Although the protein influx at 1 h was delayed by si-p97 intervention, it continued to 24 h after NM withdrawal. In the early damage, the affected pathways mainly included spliceosome, ribosome biogenesis in eukaryotes, and mRNA surveillance, which switched to protein processing in endoplasmic reticulum and energy production in presumed repair stage. Si-p97 aggravated ferroptosis, cysteine and methionine metabolism at beginning of the damage, followed by downward ranking the transcription related pathways at 24 h. NM caused DPC and H_2AX increases at 1 h. Si-p97 suppressed them at 1 h and extended the increase time to 24 h. MG132 effected similar to si-p97. Si-p97 and si-DVC1 increased the cytoplasmic level of proteasome (PSMD2). Si-DVC1 also increased the DPC content. These results suggest that NM caused a severe and rapid protein influx and crosslink in the nucleus in the early stage of injury, followed by the formation of secondary double-strand breaks. P97 was involved in the clearance of proteins in nucleus and DPC for repair, which required the participation of DVC1 and proteasome.

Highlights

Nitrogen mustard-induced protein influx into nucleus in 16HBE cell

Nitrogen mustard-induced DNA-protein cross-link

Double strand break was secondary to DNA-protein cross-link

P97 participated in protein efflux and clearance in repair stage

Introduction

Nitrogen mustards (NM), as a previous military agent(Puyo et al., 2014), is very toxic to normal tissues, such as to cause inflammatory damage of respiratory tract, skin and eye (Charkoftaki et al., 2018; Otter and D'Orazio, 2018). Besides, NM, as well as many kinds of its derivatives, are widely used in tumor chemotherapy(Liner et al., 2018; Puyo et al., 2014). All the use in military and clinic is due to that NM is a kind of bifunctional alkylating agent (BAA) with two functional N-chloroethyl groups(Larranaga and de Cozar, 2017). These two are active electrophilic alkyl groups, which can react with nucleophilic groups of DNA or protein(Loeber et al., 2009; Romero et al., 2021). Thus, NM can lead to severe damage via both genotoxicity and cytotoxicity.

Protein is one of the main target molecules in NM damage(Romero et al., 2021), and is also the major indicator reflecting cell status. On the one hand, NM can directly cross-link the protein on DNA to form DNA-protein crosslink (DPC), a type of DNA damage(Groehler et al., 2015); on the other hand, a large amount of adduction on the nucleophilic groups of the protein caused by NM can also cause cell microenvironment damage, and a variety of stress response such as inflammation(Dong et al., 2021; Malaviya et al., 2021; Trager et al., 2020) and oxidative damage(Au et al., 2015; Kumar et al., 2015). Thus, monitoring the change of protein spectra can provide a macroscopic and dynamic understanding of NM-induced injury. However, it is not clear how the protein spectrum changes with time during the progress of NM injury and what are the key factors for protein repair and clearance.

Considering that when NM damage occurs, a large number of proteins in the nucleus or cytoplasm may be damaged, and the nucleoprotein may further cross-link with DNA, which can in turn indirectly aggravate the errors of DNA replication and transcription as well as protein translation(Klages-Mundt and Li, 2017; Vaz et al., 2017), therefore, a large number of proteins urgently need to be transported and degraded to alleviate the damage caused by DPC and the stress response caused by the destruction of homeostasis. P97 (also known as VCP, Cdc48, and Ter94) belongs to the functionally highly diverse AAA+ (ATPase associated with the various cellular activities) superfamily of proteins(Hanzelmann and Schindelin, 2017). The p97 participates in many different cellular pathways involved in the regulation of protein homeostasis, membrane fusion, vesicular trafficking, and chromatin-associated functions(Huryn et al., 2019). The p97 extracts and/or disassembles the ubiquitylated substrates from membranes, chromatin, and large protein complexes(Hanzelmann and Schindelin, 2017; Rageul et al., 2019). Given the known function of p97, we speculate that it may play an important role in the repair of NM injury. However, up to now, the effects of p97 in the NM-induced damage repair, have not been reported.

Therefore, in this study, we focused on the protein spectrum after NM injury, especially the change process of nuclear protein with time. We also focused on the function of p97 on the changes of nuclear protein spectrum and DPC content after injury. Our results suggested that NM caused massive protein entering into nucleus and cross-linking with DNA to form DPC at the early stage of exposure. The accumulation of DPC led to arrested DNA replication and secondary double strand break (DSBs); further, cellular metabolic disorders occurred. P97 promoted protein efflux and DPC elimination, playing an important role in the late cell repair. The repair function of p97 was closely related to the function of proteasome and DVC1.

Materials And Methods

Cell culture and treatment

Human bronchial epithelial cell line, 16HBE was cultured in the MEM medium supplemented with 10% fetal calf serum at a seeding rate of 1×10^7 per 100-mm dish. Two days later, the cells at 70-80% confluence were treated with the NM (DB, China), which was freshly dissolved in PBS. The concentration of the NM in the culture medium was 50 μM. Cells were cultured in the NM-containing medium for 1 h,

then, half number of the cell wells were harvested and the other half continued cultured to 24 h in normal medium. For the proteasome inhibition, 2 μM of proteasome inhibitor MG132 (Selleck Chemicals, Houston, TX, USA) was added, incubated for 3 h, and then shifted to the normal culture medium.

Transient transfection

The cells with a total number of 1×10^7 were seeded onto a 100-mm cell culture dish. The next day, synthesized *DVC1* siRNA and *p97* siRNA (Invitrogen Corp., Waltham, MA, USA) were transfected to the cells with Lipofectamine2000 (Invitrogen Corp.) according to the manufacturer's protocol. The cells were treated with NM as above 2 days after the transfection.

Metabolite extraction and targeted LC-MS analysis.

The targeted LC-MS analysis of samples was performed by the BIOTREE company (Shanghai, China). Cells with or without NM or si-p97 were harvested, nuclear protein and cytoplasmic protein were separated using Nuclear and Cytoplasmic Protein Extraction Kit (Beyotime, China). Proteins were adjusted to the same concentration and hydrolyzed into peptides by Trypsin. After the detection of enzymatic hydrolysis efficiency, peptides were labeled by TMT6. Different samples were labeled with different sizes of isotopes. Labeled peptides were desalted using desalting column and acetonitrile, qualified and then separated by LS-GS in a high pH. MS (Orbitrap Fusion) was used to detect the peptides, and Proteome Discoverer (PD) (version 2.4.0.305, thermo Fisher Scientific) was used to screen the graph. The graph was analyzed by Sequest HT search engines and UniprotKB-SwissProt Database.

DPC isolation

The DPC isolation method was referred to Kiianitsa's protocol with modification(Kiianitsa and Maizels, 2013). In brief, the cells were lysed by adding DNAiso reagent (TaKaRa Bio Inc., Japan) (not to exceed 2×10^6 cells per 1 mL lysis solution). Five minutes later, nucleic acids and the DPC were precipitated by adding 0.5 volume of 100% ethanol followed by centrifugation, and the precipitate was washed twice with 75% ethanol. The precipitate was resuspended in 200 μL TE buffer or MilliQ water after completing the ethanol volatilization, and the DNA concentration was quantified.

Quantification of DNA and protein in DPC preparation

SYBR Green binds to double-stranded DNA (dsDNA) and the amount of dsDNA is proportional to the intensity of fluorescence emitted by the dye. The standard DNA from the calf thymus (Sigma-Aldrich, St. Louis, MO, USA) was serially diluted with the TE to a final concentration from 0.5 ng/μL to 8 ng/μL. The DPC sample harvested from a 100-mm dish was diluted to 1:1000. A 100 μL calf thymus DNA or DPC sample was added into each well of a 96-well plate, followed by the addition of an equal volume of SYBR Green solution (Rebio Tech. Ltd., China). After 15 min incubation in the dark, the fluorescence intensity

was measured and the DNA concentration of the DPC sample was calculated from the standard curve drawn using calf-thymus DNA(Busi, 2020).

Fluorescein isothiocyanate (FITC) stock solution in dimethylformamide was added to the DPC solution (10 μg) to the final FITC concentration of 0.1 mM and incubated at room temperature for 1 h to label the cross-linked proteins. The labeled DPC then was precipitated by 100% ethanol, washed twice with 75% ethanol, air dried, and dissolved in the TE buffer. The fluorescence strength was measured on a fluorescence spectrophotometer to quantify the level of the FITC-labeled protein. The loading amount of DPC samples could be adjusted according to the protein concentrations(Shoulkamy et al., 2012).

GST pull-down

Methods were performed according to the standard procedure. Briefly, the DVC1 plasmid was constructed into a pet-GST vector (GeneCreate, China), and the DVC1 protein with the GST flag (GST-DVC1) was expressed in the E. coli system and purified. The GST-DVC1 and the negative control (GST) were incubated with the Sepharose beads and the total protein sample of cell lysates from the different treatment groups. Solutions washed from each group were run on SDS-PAGE, and rabbit polyclonal anti-GST antibody (Santa Cruz Biotech., Dallas, TX, USA) was used to tag the Western blot. If the GST fusion protein can be detected, the mass spectrometer was used to identify the combined proteins.

Western blot

Methods were performed according to the standard procedure with the nitrocellulose membrane. Rabbit polyclonal anti-p97 antibody (Abcam, Cambridge, MA, USA), rabbit polyclonal anti-p-H_2AX antibody (Santa Cruz Biotech.), and mouse polyclonal anti-β-ACTIN antibody (Santa Cruz Biotech.) all were used at a dilution of 1:1000. The band intensity was captured and quantified. All the band intensities of the target proteins were adjusted by calculating the ratio to β-ACTIN.

Immunofluorescence

The cells were washed using PBS and then treated with 4% paraformaldehyde and 0.5% Triton X. Goat serum was used to block the unspecific binding, and rabbit polyclonal anti-PMSD2 antibody (CST) were added to incubate overnight. The FITC labeled goat-anti-rabbit secondary antibody was added to the cells the next day and DAPI was used to stain the nucleus.

Proteasome activity assay

To detect the activity of the 20S proteasome, 7-amino-4-methylcoumarin (AMC) was diluted to different concentrations (from 12.5 μM to 0.20 μM) for drawing a standard curve. Protein samples were collected from the cell lysates and adjusted to the same concentration. The proteasome substrate (Suc-LLVY-AMC) was added to the same amount of protein samples for a reaction to produce AMC. The fluorescence intensity of the AMC was detected under 380/460 nm wavelengths and the inhibition ratio of proteasome activity was calculated from the standard curve.

Statistical Analysis

All the sample sizes were at least three. In LC-MS analysis three parallel samples were mixed and Significant B algorithm(Bolstad et al., 2003) was used to screen differentiated proteins. Kyoto Encyclopedia of Genes and Genomes (KEGG) Pathway Database (www.kegg.jp/kegg/pathway.html) was used for metabolic pathway analysis. Gene Ontology Database (http://www.geneontology.org/) was used for function enrichment analysis. Other experiment data were analyzed by one-way ANOVA and presented as mean ± standard deviation. Bonferroni correction was used for the *post-hoc* test. The *P*-value less than 0.05 was considered statistically significant.

Result

NM caused cellular protein content or distribution change

NM exposure of people often causes acute damage and needs quick evacuation from contaminated sites. NM was known to cause severe cell death. Considering cell damage and repair is a dynamic process, we focused on the differences of protein expression at different time points after NM exposure, so as to correspondingly reflect the cell performance at different time points. One hour of NM treatment was used to imitate the initial stage of cell damage. Continued culture for another 24 h with normal medium after the NM treatment was used to represent the repair stage of the cells. By separately isolating proteins in nuclear and cytoplasmic compartments, the changes of protein distribution was profiled using targeted LC-MS analysis.

The relative expression level of proteins in control and NM-treated groups were calculated. By setting fold change value of 1.2 and 0.83 to represent significant up- and down-regulation of proteins after NM treatment, protein level and distribution changes were dynamically analyzed. Differential proteins whose fold change was higher than 1.2 or lower than 0.83 were analyzed further (the blue, green and purple dots in Fig. 1a). It was found that, there were more kinds of nuclear proteins up-expressed at 1 h than at 24 h (449 vs 308 in Table 1). Opposite to nuclear proteins, there were less kinds of cytoplasmic proteins up-expressed at 1 h than at 24 h (297 vs 398 in Table 1). Comparing the relative ratio of nuclear and cytoplasmic proteins at early and late time point, we found 400 proteins had a higher expression level in nucleus than that in cytoplasm at 1 h, which reduced to 347 at 24 h. However, the number of proteins which had a higher expression level in cytoplasm displayed less change at the two time points (Table 1). This indicated the kinds of nuclear proteins raised at the early stage of NM damage (1 h), but these nuclear proteins might be moved out or be cleared following the repair progression. Lots of proteins entered into nuclear may also indicate nucleus was sensitive to NM exposure.

To understand what kind of protein entered in the nucleus, we took the proteins whose fold change value were the highest (more than 10 or less than 0.25) as an example for further analysis. It was found the percentage of lysine in up-regulated proteins (14.45%) in nucleus was much higher than that in down-regulated proteins (5.72%) at 1 h (Fig. 1b). We know that the nuclear localization signals (NLS) of proteins usually consist of a single stretch of basic amino acids comprised primarily of lysine (K) and

arginine (R) residues(Dingwall and Laskey, 1991, Scalabrin et al., 2018). High lysine content might prompt active nuclear location of NSL-containing proteins. Furthermore, lysine is reported to have a nucleophilic site to crosslink with DNA(Tretyakova et al., 2015). Besides, NM is a bi-functional alkylation agent and can simultaneously alkylate DNA on its nucleophilic site, such as N7-guanine, to crosslink DNA and protein. Considering so many lysine-rich protein in nucleus, we conjectured DPC formation at the early stage of damage. Here we found NM exposure caused DPC production (Fig. 1c), which could prevent or delay the turnover of the crosslinked proteins. Besides, NM also induced large amount of H_2AX phosphorylation, indicating severe DSB existence (Fig.1d).

Table 1 change of protein distribution at different time

location	At 1 h			At 24 h		
	Increase	Decrease	High ratio	Increase	Decrease	High ratio
nucleus	449	318	400	308	328	347
cytoplasm	297	443	309	398	389	316

Note: high ratio means the extra number of differntial proteins in nucleus (or cytoplasm) than in cytoplasm (or nucleus).

Nuclear protein spectrum changes in the early stage of NM damage

Due to the main function of p97 is protein transportation and degradation, it could be involved in NM-induced damage and repair of cellular components. We used p97 siRNA to interfere its expression and further analyzed nuclear protein profile (Fig 2a). Similar protocol and threshold value of fold change with Fig. 1a were adopted for the comparison and analysis of protein profiles (Fig. 2b, 2c). The numbers of differential nuclear proteins in each two-group comparison at 1 h and 24 h were showed in Table 2. These differential proteins were expressed as up-regulation, down-regulation and total. It was found that, although the kinds of differential nuclear proteins at 24 h reduced (767 vs 636), si-p97 blockaded the decline (716 vs 712). When these proteins were classified by Venn graph, totally 171 kinds of proteins were commonly changed in all three comparison (the middle overlap in Fig. 2d,i), which meant the expression of these proteins can be significantly changed by NM, si-p97 or their combination.

When dividing the nuclear proteins into up-regulated (Fig. 2d,ii) and down-regulated (Fig. 2d,iii), the middle overlap meant that NM caused the increased or decreased level of these proteins significantly while si-p97 significantly exaggerate the changes in the same direction. Here, upon NM exposure, the 5 upregulated proteins (GFPT2, RSPH3, FSHR, BMP3, IZUMO2) and the 4 downregulated proteins (MGST1, SREBF1, TMEM19, TRMT112) were further aggravated by si-p97 treatment. The fold change of these 9 proteins showed in Fig. 2d, iv and v respectively. More interestingly, these 9 proteins were related to DNA cross-link damage and cell metabolism, suggesting these cell activities were double hit by NM and p97

defect. The rest 162 proteins (171-9=162) of the commonly changed proteins in Fig. 2d,i was reversed to different extent by si-p97, but their fold changes were still within the defined range of significance.

Table 2 differentiated protein number in NM and si-p97 treatment

range	group	1 h	24 h
total	NM vs ctrl	767	636
	si-p97+NM vs ctrl	716	712
	si-p97+NM vs NM	856	753
up-regulation	NM vs ctrl	449	308
	si-p97+NM vs ctrl	458	377
	si-p97+NM vs NM	429	381
down-regulation	NM vs ctrl	318	328
	si-p97+NM vs ctrl	258	335
	si-p97+NM vs NM	427	372

Signal pathway changes in the early stage of NM treatment

Next, we clustered all the differential proteins according to the signal pathways they belonged to using KEGG analysis in order to rule out the involved top 10 signal pathways. Compared with the normal control, the top 3 involved signal pathways in 1-hour-NM-treatment group were up-regulated spliceosome, ribosome biogenesis in eukaryotes, and mRNA surveillance pathway, as well as RNA transport (ranked 9) reflecting active DNA transcription, mRNA fidelity check and new protein synthesis. The new proteins definitely contributed to the changes of protein spectrum in the early stage of NM damage. Meanwhile, a direct and quick energy production was suppressed in terms of the down-regulated carbon metabolism, pyruvate metabolism, and pantothenate and CoA biosynthesis (ranked 12) (Fig. 3a and Table 3). The inhibition of biosynthesis of amino acids could be resulted from the reduced carbohydrate metabolism, of which the intermediate products are initial materials for amino acids synthesis.

When si-p97 was additionally introduced, the top 3 at 1 h did not change, indicating the effect of NM insult on these pathways was dominant. The active protein synthesis and suppressed energy production generally remained (Fig. 3b and Table 3). Besides, the rank promotion of ferroptosis, cysteine and methionine metabolism suggested si-p97 enhanced the oxidation stress and the abnormality of oxidative-reduction system, as well as cell death via ferroptosis caused by them. Fig. 3c showed the changes caused by si-p97 only, most of which were quite different from Fig. 3a and 3b, but did reflect the functions of p97 itself.

When clustered all the pathways, spliceosome and mRNA surveillance pathway were the two common pathways in the Venn graph (middle overlap in Fig. 3d), indicating an extra influence on the function of these pathways by p97 deficiency.

Table 3 Significant pathways at different time

Signal pathways	1 h			24 h		
	Trends	Rank		Trends	Rank	
		NM vs ctrl	si-p97+NM vs ctrl		NM vs ctrl	si-p97+NM vs ctrl
carbon metabolism	Down	**4**	**10**	Up	**2**	**3**
biosynthesis of amino acids	Down	**6**	**7**	Up	**8**	**8**
spliceosome	Up	**1**	**1**	Down	**4**	94
mRNA surveillance pathway	Up	**3**	**3**	Down	**3**	60
pentose phosphate pathway	Down	12	**8**	Up	**7**	**7**
ribosome biogenesis in eukaryotes	Up	**2**	**2**	-	84	49
protein processing in endoplasmic reticulum	Down	134	201	Up	**1**	**1**
complement and coagulation cascades	-	186	51	Up	**5**	**5**
cholesterol metabolism	-	199	155	Up	**6**	**10**
RNA transport	Up	**9**	48	Down	**10**	79
hepatocellular carcinoma	Up	**7**	24	-	249	232
Herpes simplex infection	Up	**5**	78	-	**13**	**11**
pyruvate metabolism	Down	**8**	17	Up	51	96
apoptosis	Up	**10**	128	-	58	176
Ferroptosis	Down	17	**4**	Up	**27**	197
Cysteine and methionine metabolism	Down	**14**	**5**	-	undetected	undetected
thermogenesis	Down	55	**6**	-	158	153
pantothenate and CoA biosynthesis	Down	31	**9**	-	undetected	112
one carbon pool by folate	Down	109	69	Up	**9**	117
ECM-receptor interaction	Up	228	53	Up	131	**2**
small cell lung cancer	-	56	29	Up	102	**4**
systemic lupus	Up	170	208	Up	38	**6**

erythematosus							
prion diseases	Down	73	**12**		Up	**22**	**9**

Note: Trends means proteins in the corresponding pathway were up- or down-regulated. "-" means both up- and down- regulated proteins were involved and no obvious trends can be defined. Rank reflects the significants according to *P* value. Bold means $P<0.05$ and the exact rank is significant.

Nuclear protein spectrum changes in the repair stage of NM exposure

After 1 h treatment, NM was replaced by normal medium and cells culture continued till 24 h. We used this time point to represent the repair stage after NM exposure. Table 2 showed the number of total differential nuclear proteins going downword in NM group from 1 h to 24 h (636 vs 767), indicating the cell status is turning to normal because cells were engaged in repairing at this time. However, the number of differential proteins had little change in NM+si-p97 group at different time point (712 vs 716), indicating protein did not exit from nucleus without p97.

Because the number of protein kinds are not proportional to the amount of the proteins, we tested whether more kinds of differential proteins were accompanied by more amount of the proteins that entered and/or remained in nucleus with NM or in combination with p97 deficiency. We calculated the ratio of nuclear protein to the total protein and setting the ratio in control group as 1. Both at 1 h and 24 h, the ratios were higher in NM group compared with normal control. Si-p97 further elevated the ratio at 24 h but not 1 h (Fig 4a), which indicated p97 also contribute to the more amount of protein retention in nucleus during the repair process in addition to a larger number of protein kinds (Table 2).

Compared with 1 h (Fig. 2d), numbers of differential proteins in each region in the Venn graph changed a lot at 24 h (Fig. 4b, i). Totally 52 kinds of proteins were commonly changed in all three comparison (the middle overlap in Fig. 4c,i), which meant the expression of these proteins can be significantly changed by NM, si-p97 or their combination.

When grouping the nuclear proteins as up-regulated and down-regulated as above, the middle overlap in Fig. 4b,ii and iii meant that, NM caused the level of these protein changed (both up or down) significantly, and si-p97 exaggerated the protein level changes in the same direction as NM. Here, NM and si-p97 synergistically upregulated 18 proteins (H2AX, MRM3, H2BC13, HIST3H2A, AREG, APOE, LAMP2, HIST2H2AC, HBA1, HIST2H2AB, ATF3, S100A9, IGLC2, SNAPC4, LYZ, GPX3, ANP32C, RPIA) (Fig. 4c, ii,iv), and downregulated of other 11 proteins (EHD2, PDK1, CRIP2, CLP1, MT-ND4, ANGPTL4, IREB2, KAT8, TOR1AIP2, SLC25A15, SLC35F6) (Fig. 4c, iii,v).

Signal pathway changes in the repair stage of NM exposure

We also clustered all the differential nuclear proteins at 24 h after NM treatment using KEGG analysis as before. Opposite to cell performance at 1 h, the protein synthesis was suppressed and energy production was enhanced as indicated by the down-regulated mRNA surveillance pathway, spliceosome, and RNA transport, and the up-regulated carbon metabolism, pentose phosphate pathway, one carbon pool by

folate, respectively (Fig. 5a and Table 3). From this point of view, it was easy to understand that cells were in a quite different situation at 1 h and 24 h. The top 1 KEGG pathways in NM group was protein processing in endoplasmic reticulum. The upregulated biosynthesis of amino acids could be a result of abundant material supply from carbohydrate metabolism. The meaning of complement and coagulation cascades, and cholesterol metabolism was not clear (Fig. 5a).

In NM+si-p97 group, the inhibition on transcription was alleviated as suggested by the downward ranking of mRNA surveillance pathway (dropped from 3 in NM group to 60), spliceosome (from 4 to 94), and RNA transport (from 10 to 79). Carbohydrate metabolism remained up-regulated as in NM group. The pathways of protein processing in endoplasmic reticulum, complement and coagulation cascades, and cholesterol metabolism kept in the top 10 list. ECM-receptor interaction, The significance of related to small cell lung cancer, systemic lupus erythematosus, and prion diseases was not understood (Fig. 5b).

Fig. 5c showed the top 10 pathways only influenced by si-p97, which indicated p97 was functioned in these aspects in damage repair stage.

P97 regulated DNA damage in NM exposure

DPC causes DNA replication stress and induce DSB, which can be visualized by H_2AX phosphorylation. As the greatest fold change of H_2AX was revealed in si-p97 plus NM treatment at 24 h (Fig. 4c,ii,iv), we presumed p97 play an important role in DNA damage repair. Considering more nuclear proteins could provide a higher opportunity of DNA cross-linking with protein via MN alkylation, the levels of DPC and H_2AX with or without si-p97 intervention were compared. Consistent with Fig.1d, NM raised the levels of DPC (Fig.6a) and H_2AX (Fig.6b) with a higher level at 1h than that at 24 h, supporting the idea that setting damage and repair stage respectively at these time points. However, compared with NM group, si-p97 caused additional DPC formation only at 24 h but not at 1 h (Fig.6a), which proposed an important role of p97 in the repair of DPC, and was supported by a consistent extra increase of H_2AX at 24 h by si-p97 introduction (Fig. 6b). More interestingly, NM-enhanced p-H_2AX expression at 1 h was suppressed in the present of si-p97 (Fig. 6b), which was verified by Western blot (Fig. 6c). These data supported the idea that DPC-induced DSB was secondary to DPC clearance, i.e., a step following the digestion of large adducted protein and the cut off of the residual protein or together with the crosslinked base. It should be mentioned that NM exposure did not influence p97 expression at both 1 h and 24 h (Fig. 6c).

P97 interacted with proteasome in NM exposure

Considering one of the function of p97 was presenting protein to proteasome for degradation, we detected the damage when proteasome was inhibited. Although NM produced high p-H_2AX level at 1 h, the addition of treatment with MG132, the inhibitor of proteasome, partially prevent the increase of p-H_2AX (Fig. 7a). MG132 displayed a little, if any, inhibitory effect on the removal of NM-induced DPC at 24 h (Fig. 7b). These results were similar to the effect of si-p97 transfection, indicating p97 was coordinated with proteasome in both NM damage and repair. To find the most active part of proteasome in NM and si-

p97 treatment, we analyzed all the subunits that LC-MS detected. There were 45 proteasome subunits at 1 h and 42 subunits at 24 h detected. Among all of the subunits, the expression of PSMD2 in whole cell was the highest. In addition, the expression of PSMD2 obviously increased in the present of si-p97 (dot line box in Fig. 7c and 7d). The coordination between p97 and PSMD2 was also detected further by immunofluorescent staining. The expression of PSMD2 remarkably up-regulated and mainly concentrated in nucleus after NM treatment, while si-p97 intervention raised PSMD2 content in cytoplasm (Fig. 7e). We speculated that more proteasomes were recruited to nucleus to process unwanted proteins, such as proteins in DPC, to repair the NM injury, and loss of p97 could partially reduce nuclear loading of proteasome and inhibit protein degradation.

P97 interacted with protease DVC1 in nuclear proteolysis

Previous results had proved DVC1, a kind of protease, taken part in DPC repair, so we were interested in the relationship between DVC1 and p97. Our result was consistent with Davis'(Davis et al., 2012) that, p97 physically interacted with DVC1 in in vitro assay (Fig.8a). To find more cooperators of DVC1, LC-MS was used to detect the proteins pulled down by GST-DVC1. Coincidentally, besides p97, PSMD2 was also the interacted protein of DVC1 (Table 4). Thus, we detected the influence of DVC1 on PSMD2 and proteasome. In si-DVC1+NM treated group, the expression of PSMD2 was maintained in high level as in NM group, but the location of PSMD2 was in both nucleus and cytoplasm (Fig. 8b), suggesting less proteasome was recruited to nucleus. The activity of proteasome decreased after si-DVC1 treatment (Fig. 8c), meanwhile, DPC formation obviously increased (Fig. 8d), similarly with si-p97 or MG132 treatment. These data together demonstrated the cooperation of P97, DVC1 and proteasome in DPC repair after NM damage.

Table 4 Pathways and proteins captured by DVC1 in KEGG cluster analysis

Term	Count	P-Value	Top10 Genes
Spliceosome	9	1.56E-04	SRSF3, SF3B1, U2AF2, TRA2B, DHX15, DDX5, RBMX, PUF60, RBM25
Glycolysis/Gluconeogenesis	6	9.47E-04	PGM2, LDHB, PGM1, PGAM1, ALDH2, PGK1
Biosynthesis of antibiotics	10	0.00104	PGM2, SDHA, LDHB, IDH3G, PGM1, PGAM1, ALDH2, PGK1, OAT, IDH3A
Non-homologous end-joining	3	0.010426	XRCC5, XRCC6, FEN1
Carbon metabolism	6	0.011812	SDHA, IDH3G, TKFC, PGAM1, PGK1, IDH3A
Peroxisome	5	0.017999	ECH1, GSTK1, PRDX5, ACSL3, PRDX1
Proteasome	4	0.018027	PSME2, PSMD1, PSMD2, PSMA8
Arginine and proline metabolism	4	0.020189	CNDP2, P4HA1, ALDH2, OAT
Citrate cycle (TCA cycle)	3	0.050925	SDHA, IDH3G, IDH3A
Biosynthesis of amino acids	4	0.056684	IDH3G, PGAM1, PGK1, IDH3A
Base excision repair	3	0.063679	HMGB1, PARP1, FEN1
Fatty acid degradation	3	0.088207	ALDH2, ACSL3, CPT1A

Discussion

Nitrogen mustard is classified as vesicant in military applications(Ghabili et al., 2010). It caused tissue erosion through multiple mechanisms(Malaviya et al., 2021), which might be related to its molecular structure. Due to the bi-functional alkylation, its target is not limited to a specific molecule, but presents a wide range, that is all the molecules with nucleophilic groups(Steinritz et al., 2021). Therefore, important components of cells, from DNA bases to proteins, can be directly or indirectly damaged. Take protein as the core, these damages can induce each other, because on the one hand, proteins can cross-link with DNA to form DPC, resulting in DNA damage, on the other hand, the damaged protein and DPC leaded to cell structure and function disorder directly and indirectly(Yue et al., 2014). Therefore, understanding how the protein spectrum changes can reflect how cells respond to NM damage. In this study, the 1 h and 24 h time points were selected to reflect the stress changes of cells after acute NM exposure and disengagement from exposure for a period of time, respectively, so as to speculate the repair process of cells in more detail. At the same time, proteomics can be used to understand the effects of damage and repair at the overall level.

We found that the content change of nuclear protein with time was greater than that of cytoplasmic protein in the process of exposure. In particular, during acute injury, a large amount of protein entered the

nucleus, especially those rich in lysine (Fig. 1b), resulting in a significant content change, but after cell was away from the injury, nuclear protein efflux appeared (Table 1), suggesting that during acute exposure, it mainly caused strong intra-nuclear damage, and the nucleus was the most sensitive site for NM injury. Therefore, we will focus our subsequent observation on nuclear proteins. Various kinds of nuclear proteins are functioning around DNA to ensure the normal actions of DNA such as chromatin modeling, replication, transcription and DNA repair. Normally, these proteins are recruited transiently to DNA only when needed, and released from DNA and/or protein complex after fulfill their physiological functions. Alkylating agents like NM can cause the alkylation of DNA and proteins to form DPC by its two N-chloroethyl groups. Our results also confirmed that NM damage caused an increase in DPC content (Fig. 1c). If the proteins on these DPCs were that had existed in the nucleus before NM damage, only the DPC content would increase, without a large kinds of protein entering the nucleus after 1 h exposure. Therefore, our results suggested that the proteins in DPC are not only inherently present in the nucleus, but also partially including those which entered the nucleus but be cross-linked to the DNA chain by NM when exposing. This may be because NM itself can directly adduct to a protein with one chloroethyl group first, and then enter into the nucleus with the adducted protein and further cross-linked with DNA strand with another chloroethyl group.

We were very concerned about how a large number of nuclear proteins exited from 1 h to 24 h. It has been reported that the functions of p97 included chromatin protein removal, endoplasmic reticulum mediated protein degradation and membrane fusion(Kustermann et al., 2018, Stach and Freemont, 2017). P97 can capture the target protein, and then, depending on energy generation via ATP hydrolysis by its D domain, the structure of p97 transformed, which drives the target protein to pass through the circular D domain, so that the target protein can be extracted from its original position (such as chromatin, etc.)(Bodnar and Rapoport, 2017, Hanzelmann and Schindelin, 2017). At the same time, the spatial structure of the target protein is changed, making it more easily degraded(Bodnar and Rapoport, 2017). Our previous studies have confirmed that p97 can remove MGMT protein crosslinked with DNA(Cheng et al., 2016). Therefore, we speculated that the large amount of protein in nucleus in this experiment needed the help of p97 in efflux at 24 h.

In proteomics analysis, NM vs. ctrl meant the influence caused only by NM, si-p97+NM vs ctrl meant the influence of p97 deficiency in the condition of NM damage, while si-p97+NM vs NM can be thought as the influence of si-p97 itself. At 1 h, the total number of differential nuclear protein in NM intervention was more than that in NM combined with si-p97 (Table 2, Fig. 2d), but at 24 h, this situation was reversed, i.e., the total number of differential nuclear protein in NM+si-p97 intervention was more than that of NM alone (Table 2, Fig. 4b). This phenomenon was partly similar when the up-regulated and down-regulated proteins were analyzed separately (Table 2, Fig. 2d and 4b). Considering differential protein reflects a change away from normal, i.e., there should be no differential proteins in normal condittion, the result suggested that p97 deletion might not be the main factor for aggravating the damage at the early stage of exposure, but the effect of p97 on nuclear protein might be reflected in the repair stage after NM withdrawal. At the same time, we are also noticed that si-p97 itself also causes a large number of

differential protein (si-p97+NM vs NM), but most of the proteins have no overlap with other groups on Venn graph, which indicated the effect caused by p97 deficiency was different from NM.

Cluster analysis of proteome revealed that NM mainly affected the upstream process of cellular material metabolism through several pathways such as spliceosome, ribosome biogenesis and mRNA surveillance during acute injury (Fig. 3), which might be due to the rapid stress response by NM injury on DNA in the early stage, for example, the formation of DPCs induced stress on shearing, transcription and translation(Morocz et al., 2017). P97 inhibition would further enhance the redox stress and aggravate tissue damage. However, in the repair period, the sequences of significant signal pathways were significantly reranked. NM was removed, however, the DNA damage may had effected on the downstream already. Thus, the changes at this time are mainly concentrated on the downstream of some specific metabolic processes of various substances (Fig. 5). Most of the downreguleted proteins in Fig. 4b,iii,v are also involved in metabolic process, indicating a very complex regulation or even disorders in metabolism, which may be the late effect of acute DNA damage. Protein processing in endoplasmic reticulum ranked first. Although it was difficult to explain how the proteins in this pathway entered nucleus, these proteins may be involved in p97-related protein removal, for it was reported that p97 can presented proteins from chromatin to endoplasmic reticulum for degradation(Stach and Freemont, 2017).

NM also caused DSB (Fig.1d), a severe DNA damage, consistent with previous reports(Jan et al.). However, there was no experimental confirmation about the relationship among various NM-induced DNA damage. Our experiment found that NM can cause DPC and DSB in 1 h, but when p97 was inhibited, although the DPC increased, the DSB level (marked by p-H2AX) did not significantly increase in the early stage (1 h). After 24 h, DPC and DSB increased significantly even in the absence of p97. Similar with H_2AX, many up-regulated proteins in Fig. 4b ii,iv are also histone related proteins and were also increased only at 24 h. This result was very interesting. According to the structure of NM, it can cause DPC or DNA strand cross-linking through two chloroethyl arms(Singh et al., 2018), but it was unreasonable to cause DSB directly. We suspected that the increase of DSB in NM group in 1 h might be due to the replication pressure caused by both DPC and DNA strand cross-linking. When p97 was deleted, no more protein was nucleated at the early stage (Fig.4a and Table 2), so that DPC level was not higher than that of NM caused alone (Fig. 6a), which partially offset the influence on replication pressure and DSB formation (Fig. 6b, 6C)(Swan et al., 2021). As time went on, the p97 deletion led to a large number of protein aggregation in the nucleus, and DPC could not be cleared. When DNA replicated, because DPC still exists in large quantities, a large number of cross-linked proteins on DNA strand led to the increase of replication pressure, which caused DSB. This also indicated that DSB is secondary to DPC as the injury progresses.

MG132 also suppressed the p-H2AX level in the initial stage (Fig. 7a), which was similar to the result of si-p97 treatment, suggesting that proteasome had a similar effect to p97, which might inhibit protein entering into nucleus in the initial stage of NM exposure. However, proteasome inhibition also caused a slower DPC clearance with time(Ortega-Atienza et al., 2015). We found that the PSMD2 level increased after NM injury (Fig. 7c-e).PSMD2 was a subunit ubiquitin receptor of proteasome 26S, participating in

proteasome function by encoding one of the non-ATPase subunits of the 19S regulator lid(Ying et al., 2022), suggesting that more target proteins needed to be degraded. Besides, High PSMD2 expression may indicate a risk of abnormal cell proliferation and cell cycle progression, even a poor cancer prognosis(Li et al., 2018, Salah Fararjeh et al., 2021), so the concentration of PSMD2 near the nucleus in NM injury may also indicate a genomic instability. However, when p97 was deleted, PSMD2 was scattered in the whole cell, indicating removing nuclear protein was not the main task.

P97 can recognize and transport multiple target proteins from chromatin, endoplasmic reticulum, and membrane because it contains an N-domain that can bind with ubiquitin ligases. Therefore, p97 can capture ubiquitinated proteins through interaction with ubiquitin ligases(Limanaqi et al., 2020, Stach and Freemont, 2017). Our previous studies have confirmed that the removal of DNA-crosslinked MGMT protein is ubiquitination-dependent. Previous reports(Mosbech et al., 2012) suggested that DVC1 was involved in the process of nuclear protein presentation to p97. DVC1 was a protease that recognized the target protein(Reinking et al., 2020) to be degraded on DNA through the ubiquitin-binding domain(Morocz et al., 2017) and presented it to p97. Our experiment confirmed that DVC1 could directly recognize p97 (Fig. 8a). Similar to p97, DVC1 can also bind to PSMD2, and, the distribution of PSMD2 tends to the whole cell rather than concentrating on the nuclear region after DVC1 deletion. At the same time, the activity of proteasome was decreased, and the content of DPC was increased, suggesting that inhibition of DVC1 also hindered the degradation of nuclear protein by interfering proteasome (Table 4, Fig. 8b, c). DVC1 may form a complex with p97 and proteasome, and participate in the process of removing nuclear protein together. According to the domains of DVC1 and p97, and the results of this study, we believed that the clearance of nuclear protein by p97 is DVC1-dependent.

To sum up, this study found that NM caused a large number of proteins enter into nucleus and cross-link with DNA to form DPC in the early stage of exposure. The accumulation of DPC leaded to the obstruction of replication, transcription and translation, and leaded to secondary DSB, which further leaded to the disorder of energy metabolism. P97 promoted protein efflux from nucleus and eliminating DPC, which played an important role in cell repair. The repairing effect of p97 was closely related to proteasome and DVC1. In this study, the process of p97 on precisely removing a specific nucleoprotein in the dependence of DVC1 had not been deeply studied, and further research is needed.

Abbreviations

NM, nitrogen mustard

BAA, bifunctional alkylating agent

DPC, DNA-protein cross-link

DSB, double strand break

Declarations

Grant Support

Young Talent Cultivation Program of Military Medical Science and Technology, PLA (grant number 20QNPY001); Young Talent Cultivation Program of Army Medical University (grant number 2018XQN03)

Ethics approval

Not applicable.

Authors' contributions

All authors contributed to the study conception and design. Material preparation, data collection, analysis were performed by Jin Cheng, Wenpei Yu, Haoyin Liu and Xunhu Dong. The first draft of the manuscript was written by Jin Cheng. The experiment performance was guided by Yan Sai and Feng Ye. Statistical analysis was performed by Guorong Dan, Mingliang Chen, Yuanpeng Zhao and Xi Zhang. Zhongmin Zou helped with manuscript reviewing and editing. All authors commented on previous versions of the manuscript. All authors read and approved the final manuscript.

Funding

This work was supported by the Young Talent Cultivation Program of Military Medical Science and Technology, PLA (grant number 20QNPY001), and the Young Talent Cultivation Program of Army Medical University (grant number 2018XQN03).

Availability of data and materials

The datasets generated during and/or analysed during the current study are not publicly available, but are available from the corresponding author on reasonable request.

Conflict of interest

The authors declare that there are no conflict of interest.

References

1. Au, L. et al., 2015. Suppression of Hyperactive Immune Responses Protects against Nitrogen Mustard Injury. J Invest Dermatol, 135(12): 2971-2981.
2. Bodnar, N., Rapoport, T., 2017. Toward an understanding of the Cdc48/p97 ATPase. F1000Res, 6: 1318.
3. Bolstad, B.M., Irizarry, R.A., Astrand, M., Speed, T.P., 2003. A comparison of normalization methods for high density oligonucleotide array data based on variance and bias. Bioinformatics, 19(2): 185-93.
4. Busi, F., 2020. Fluorescent Oligonucleotide Probes for the Quantification of RNA by Real-Time qPCR. Methods Mol Biol, 2113: 263-280.

5. Charkoftaki, G., Jester, J.V., Thompson, D.C., Vasiliou, V., 2018. Nitrogen mustard-induced corneal injury involves the sphingomyelin-ceramide pathway. Ocul Surf, 16(1): 154-162.
6. Cheng, J. et al., 2016. Bifunctional alkylating agent-mediated MGMT-DNA cross-linking and its proteolytic cleavage in 16HBE cells. Toxicol Appl Pharmacol, 305: 267-273.
7. Davis, E.J. et al., 2012. DVC1 (C1orf124) recruits the p97 protein segregase to sites of DNA damage. Nat Struct Mol Biol, 19(11): 1093-100.
8. Dingwall, C., Laskey, R.A., 1991. Nuclear targeting sequences--a consensus? Trends Biochem Sci, 16(12): 478-81.
9. Dong, X. et al., 2021. Vitamin D3 ameliorates nitrogen mustard-induced cutaneous inflammation by inactivating the NLRP3 inflammasome through the SIRT3-SOD2-mtROS signaling pathway. J Mol Neurosci, 11(2): e312.
10. Ghabili, K., Agutter, P.S., Ghanei, M., Ansarin, K., Shoja, M.M., 2010. Mustard gas toxicity: the acute and chronic pathological effects. J Appl Toxicol, 30(7): 627-43.
11. Groehler, A.S., Villalta, P.W., Campbell, C., Tretyakova, N.Y., 2015. Covalent DNA-Protein Cross-linking by Phosphoramide Mustard and Nornitrogen Mustard in Human Cells. Chem Res Toxicol.
12. Hanzelmann, P., Schindelin, H., 2017. The Interplay of Cofactor Interactions and Post-translational Modifications in the Regulation of the AAA+ ATPase p97. Front Mol Biosci, 4: 21.
13. Huryn, D.M., Kornfilt, D.J.P., Wipf, P., 2019. p97: An Emerging Target for Cancer, Neurodegenerative Diseases, and Viral Infections. J Med Chem.
14. Jan, Y.H., Heck, D.E., Laskin, D.L., Laskin, J.D., DNA damage signaling in the cellular responses to mustard vesicants. (1879-3169 (Electronic)).
15. Kiianitsa, K., Maizels, N., 2013. A rapid and sensitive assay for DNA-protein covalent complexes in living cells. Nucleic Acids Res, 41(9): e104.
16. Klages-Mundt, N.L., Li, L., 2017. Formation and repair of DNA-protein crosslink damage. Sci China Life Sci, 60(10): 1065-1076.
17. Kumar, D. et al., 2015. Nitrogen mustard exposure of murine skin induces DNA damage, oxidative stress and activation of MAPK/Akt-AP1 pathway leading to induction of inflammatory and proteolytic mediators. Toxicol Lett, 235(3): 161-71.
18. Kustermann, M. et al., 2018. Loss of the novel Vcp (valosin containing protein) interactor Washc4 interferes with autophagy-mediated proteostasis in striated muscle and leads to myopathy in vivo. Autophagy, 14(11): 1911-1927.
19. Larranaga, O., de Cozar, A., 2017. Mono- and Di-Alkylation Processes of DNA Bases by Nitrogen Mustard Mechlorethamine. 18(23): 3390-3401.
20. Li, Y. et al., 2018. PSMD2 regulates breast cancer cell proliferation and cell cycle progression by modulating p21 and p27 proteasomal degradation. Cancer Lett, 430: 109-122.
21. Limanaqi, F. et al., 2020. Cell-Clearing Systems Bridging Repeat Expansion Proteotoxicity and Neuromuscular Junction Alterations in ALS and SBMA. Int J Mol Sci, 21(11).

22. Liner, K., Brown, C., McGirt, L.Y., 2018. Clinical potential of mechlorethamine gel for the topical treatment of mycosis fungoides-type cutaneous T-cell lymphoma: a review on current efficacy and safety data. Drug Des Devel Ther, 12: 241-254.
23. Loeber, R.L. et al., 2009. Proteomic analysis of DNA-protein cross-linking by antitumor nitrogen mustards. Chem Res Toxicol, 22(6): 1151-62.
24. Malaviya, R. et al., 2021. Pulmonary injury and oxidative stress in rats induced by inhaled sulfur mustard is ameliorated by anti-tumor necrosis factor-alpha antibody. Toxicol Appl Pharmacol, 428: 115677.
25. Morocz, M. et al., 2017. DNA-dependent protease activity of human Spartan facilitates replication of DNA-protein crosslink-containing DNA. Nucleic Acids Res, 45(6): 3172-3188.
26. Mosbech, A. et al., 2012. DVC1 (C1orf124) is a DNA damage-targeting p97 adaptor that promotes ubiquitin-dependent responses to replication blocks. Nat Struct Mol Biol, 19(11): 1084-92.
27. Ortega-Atienza, S., Green, S.E., Zhitkovich, A., 2015. Proteasome activity is important for replication recovery, CHK1 phosphorylation and prevention of G2 arrest after low-dose formaldehyde. Toxicol Appl Pharmacol, 286(2): 135-41.
28. Otter, J., D'Orazio, J.L., 2018. Toxicity, Blister Agents (Mustard, Vesicants, Hd, Hn1-3, H), StatPearls. StatPearls Publishing
29. StatPearls Publishing LLC., Treasure Island (FL).
30. Puyo, S., Montaudon, D., Pourquier, P., 2014. From old alkylating agents to new minor groove binders. Crit Rev Oncol Hematol, 89(1): 43-61.
31. Rageul, J., Weinheimer, A.S., Park, J.J., Kim, H., 2019. Proteolytic control of genome integrity at the replication fork. DNA Repair (Amst): 102657.
32. Reinking, H.K. et al., 2020. DNA Structure-Specific Cleavage of DNA-Protein Crosslinks by the SPRTN Protease. Mol Cell, 80(1): 102-113 e6.
33. Romero, A. et al., 2021. Toxicology of Blister Agents: Is Melatonin a Potential Therapeutic Option? Diseases, 9(2).
34. Salah Fararjeh, A., Al-Khader, A., Al-Saleem, M., Abu Qauod, R., 2021. The Prognostic Significance of Proteasome 26S Subunit, Non-ATPase (PSMD) Genes for Bladder Urothelial Carcinoma Patients. Cancer Inform, 20: 11769351211067692.
35. Scalabrin, M., Dixit, S.M., Makshood, M.M., Krzemien, C.E., Fabris, D., 2018. Bifunctional cross-linking approaches for mass spectrometry-based investigation of nucleic acids and protein-nucleic acid assemblies. Methods, 144: 64-78.
36. Shoulkamy, M.I. et al., 2012. Detection of DNA-protein crosslinks (DPCs) by novel direct fluorescence labeling methods: distinct stabilities of aldehyde and radiation-induced DPCs. Nucleic Acids Res, 40(18): e143.
37. Singh, R.K., Kumar, S., Prasad, D.N., Bhardwaj, T.R., 2018. Therapeutic journery of nitrogen mustard as alkylating anticancer agents: Historic to future perspectives. European Journal of Medicinal

Chemistry, 151: 401-433.

38. Stach, L., Freemont, P.S., 2017. The AAA+ ATPase p97, a cellular multitool. Biochem J, 474(17): 2953-2976.
39. Steinritz, D. et al., 2021. Alkylated epidermal creatine kinase as a biomarker for sulfur mustard exposure: comparison to adducts of albumin and DNA in an in vivo rat study. Archives of Toxicology, 95(4): 1323-1333.
40. Swan, R.L., Cowell, I.G., Austin, C.A., 2021. A role for VCP/p97 in the processing of drug-stabilised TOP2-DNA covalent complexes. Mol Pharmacol.
41. Trager, M.H., Chen, C., Husain, S., Geskin, L.J., 2020. Nitrogen mustard gel-induced inflammation triggers lymphomatoid papulosis in patients with mycosis fungoides. J Dermatol, 47(5): 546-550.
42. Tretyakova, N.Y., Groehler, A.t., Ji, S., 2015. DNA-Protein Cross-Links: Formation, Structural Identities, and Biological Outcomes. Acc Chem Res, 48(6): 1631-44.
43. Vaz, B., Popovic, M., Ramadan, K., 2017. DNA-Protein Crosslink Proteolysis Repair. Trends Biochem Sci, 42(6): 483-495.
44. Ying, K. et al., 2022. Diverse Ras-related GTPase DIRAS2, downregulated by PSMD2 in a proteasome-mediated way, inhibits colorectal cancer proliferation by blocking NF-kappaB signaling. Int J Biol Sci, 18(3): 1039-1050.
45. Yue, L. et al., 2014. Abundance of four sulfur mustard-DNA adducts ex vivo and in vivo revealed by simultaneous quantification in stable isotope dilution-ultrahigh performance liquid chromatography-tandem mass spectrometry. Chem Res Toxicol, 27(4): 490-500.

Figures

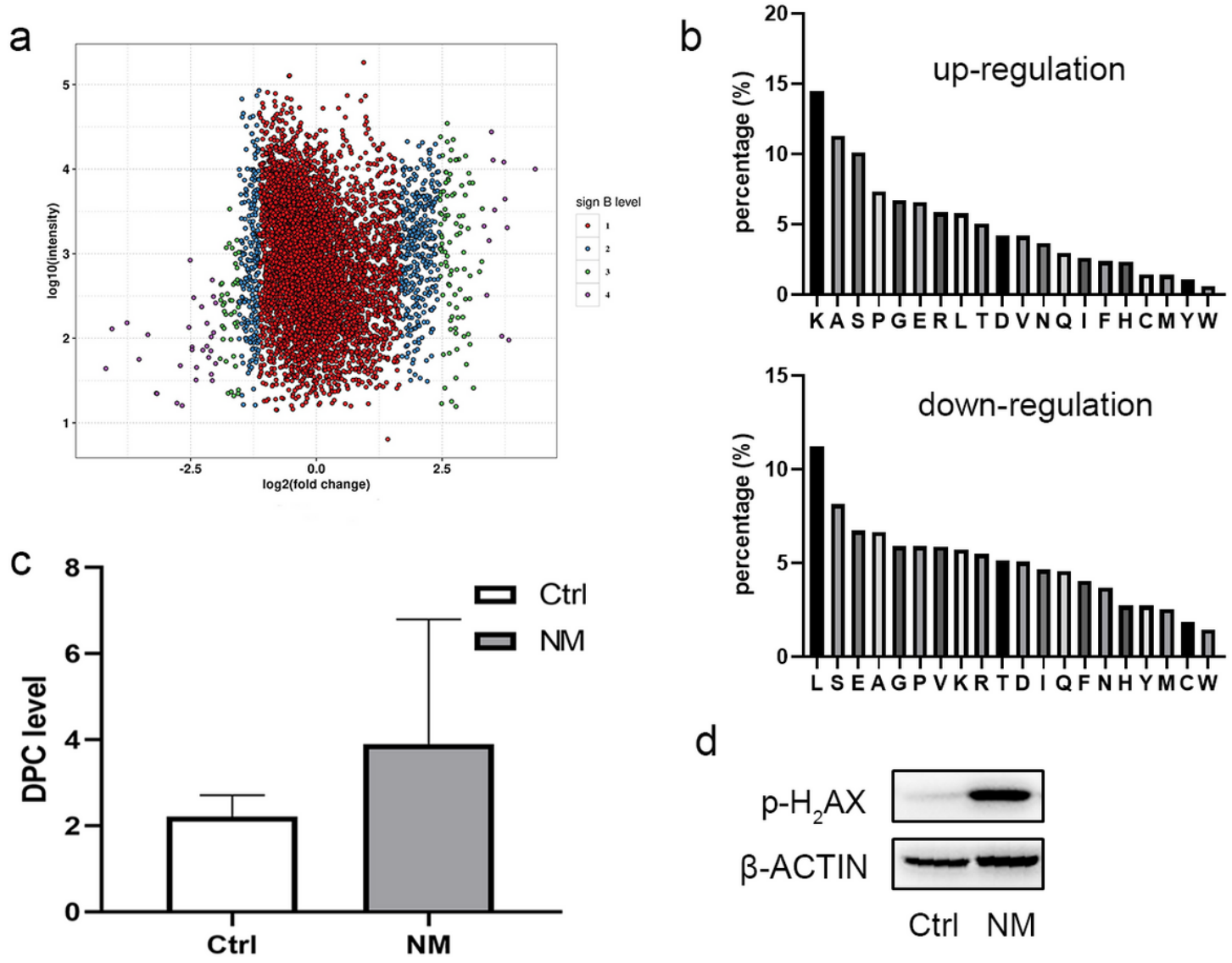

Figure 1

The impacts of NM exposure on protein expression and distribution as well as DNA damage in cells. (a) take the nuclear protein at 1 h NM treatment as an example to explain the spectrum change. the expression levels of nuclear proteins in NMgroups and control were compared pairwise, with the abscissa representing the multiple change of proteins in this comparison (the logarithm with 2 as the base), the ordinate representing the information of the expression content of proteins(the logarithm with 10 as the base), the blue, green and purple dotsrepresenting the final screening result (fold change>=1.2 or <=0.83), and the non-significant proteins was shown in red. (b) the percentages of amino acids in up- and down-regulated nuclear protein 1 h after NM treatment (c) the DPC content after NM treatment. (d) p-H2AX expression after NM treatment.

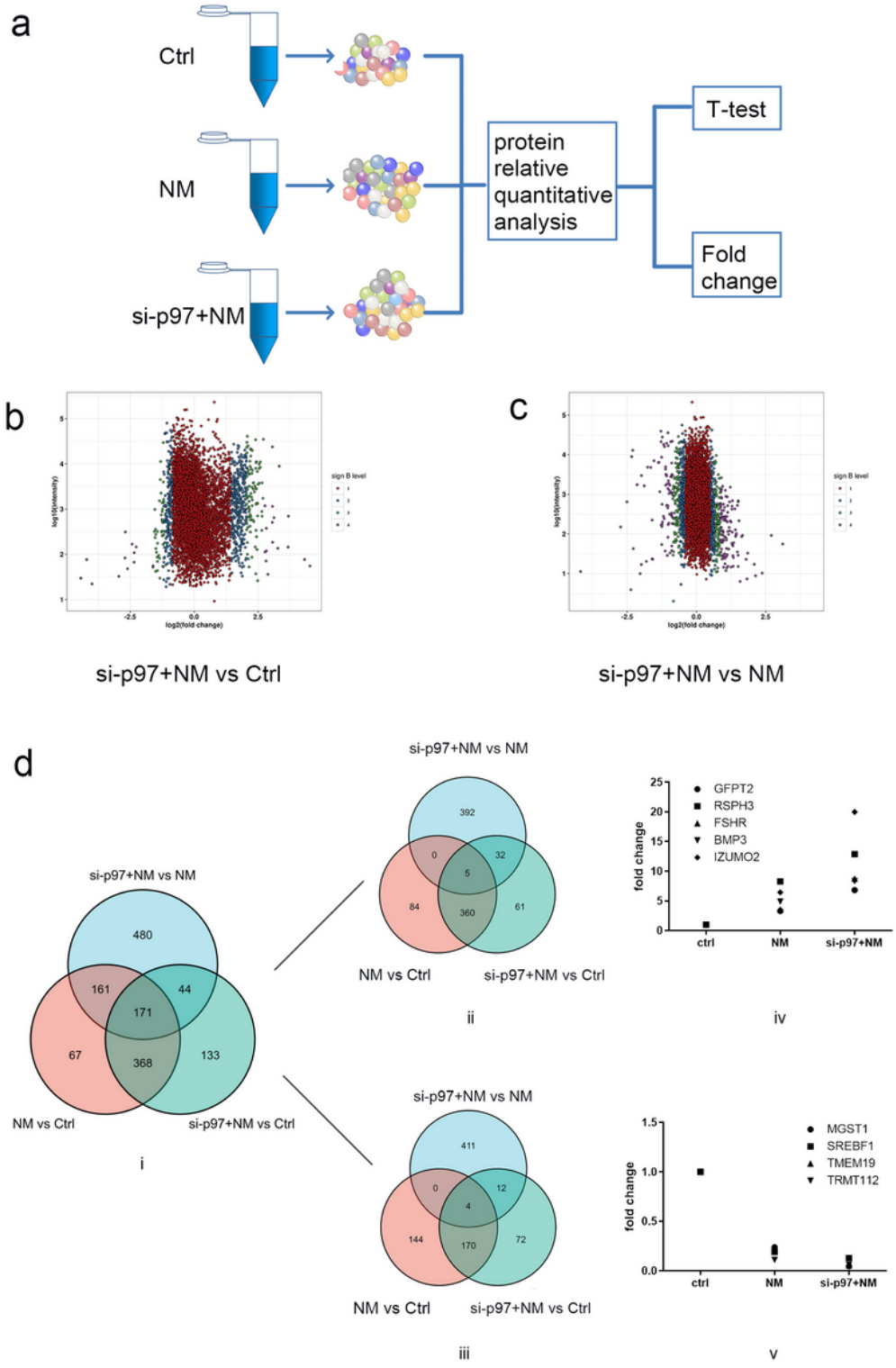

Figure 2

Overall changes of nuclear protein after 1 h of NM damage. (a) Diagram of the steps of tandem mass tags proteome quantitative detection. The nuclear protein and cytoplasmic protein were extracted from the three samples after treatment, and the expression differences were compared after quantitative analysis. (b-c) The same as Fig. 1A, after 1 h of NM treatment, the expression levels of nuclear proteins in NM and NM+si-p97groups were compared pairwise, with the abscissa representing the multiple change

of proteins in this comparison (the logarithm with 2 as the base), the ordinate representing the information of the expression content of proteins(the logarithm with 10 as the base), the blue, green and purple dotsrepresenting the final screening result (fold change>=2), and the non-significant proteins was shown in red. (d) i: The results of the pairwise comparison of the three groups, and the numbersof nuclear differential proteins at 1 h were shown using Venn graph. The red circle represented the differential proteins of NM treatment compared with the control group, which represented the effect of NM. The green circle represents the differential proteins between the si-p97+NM treatment and the control, which represented the effect of si-p97 on NM exposure. The blue circle represented the differential proteins of si-p97+NM compared with the NM group, which represented the effect of si-p97 itself without considering NM. ii-iii: The up-regulated and down-regulated proteins at 1 h in the nucleus were classified by Venn diagram separately. ii:up-regulated protein, iii: down-regulated protein. iv-v: the exact proteins and their fold changes in the middle part of Venn graph in ii and iii.

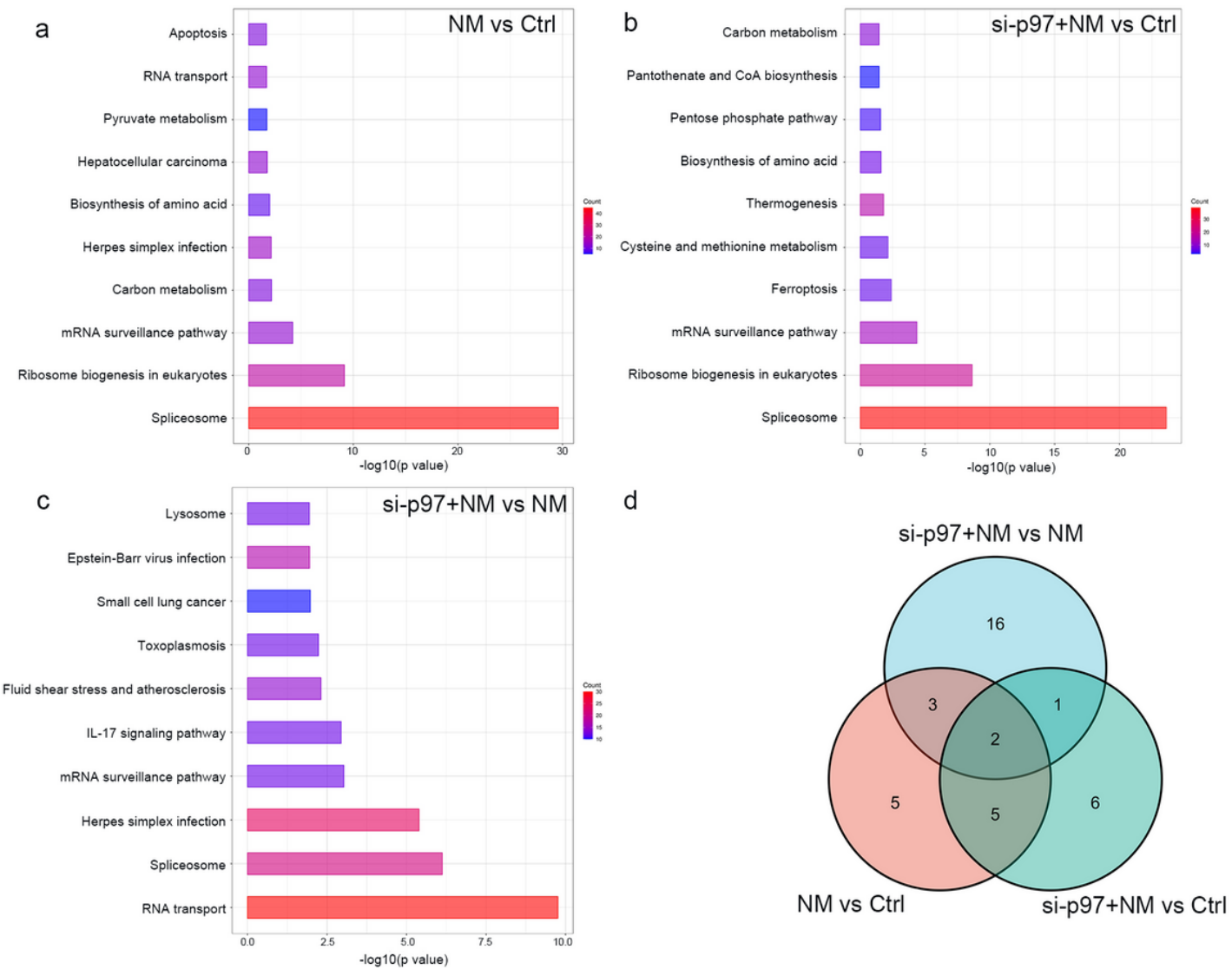

Figure 3

KEGG clustering of differential proteins in the nucleus 1 h after NM injury. (a-c) After 1 h of NM treatment, the differential proteins of the three groups were compared in pairs and sequenced into the top 10 pathways after KEGG clustering. The abscissa was -log10(p value), and the ordinate was the name of the pathway. Among them, the longer column indexed the smaller p-value, and the redder column indexed the more differentially expressedproteins in this pathway. (d) Venn graph showed the number of all the significant pathways by KEGG clustering.

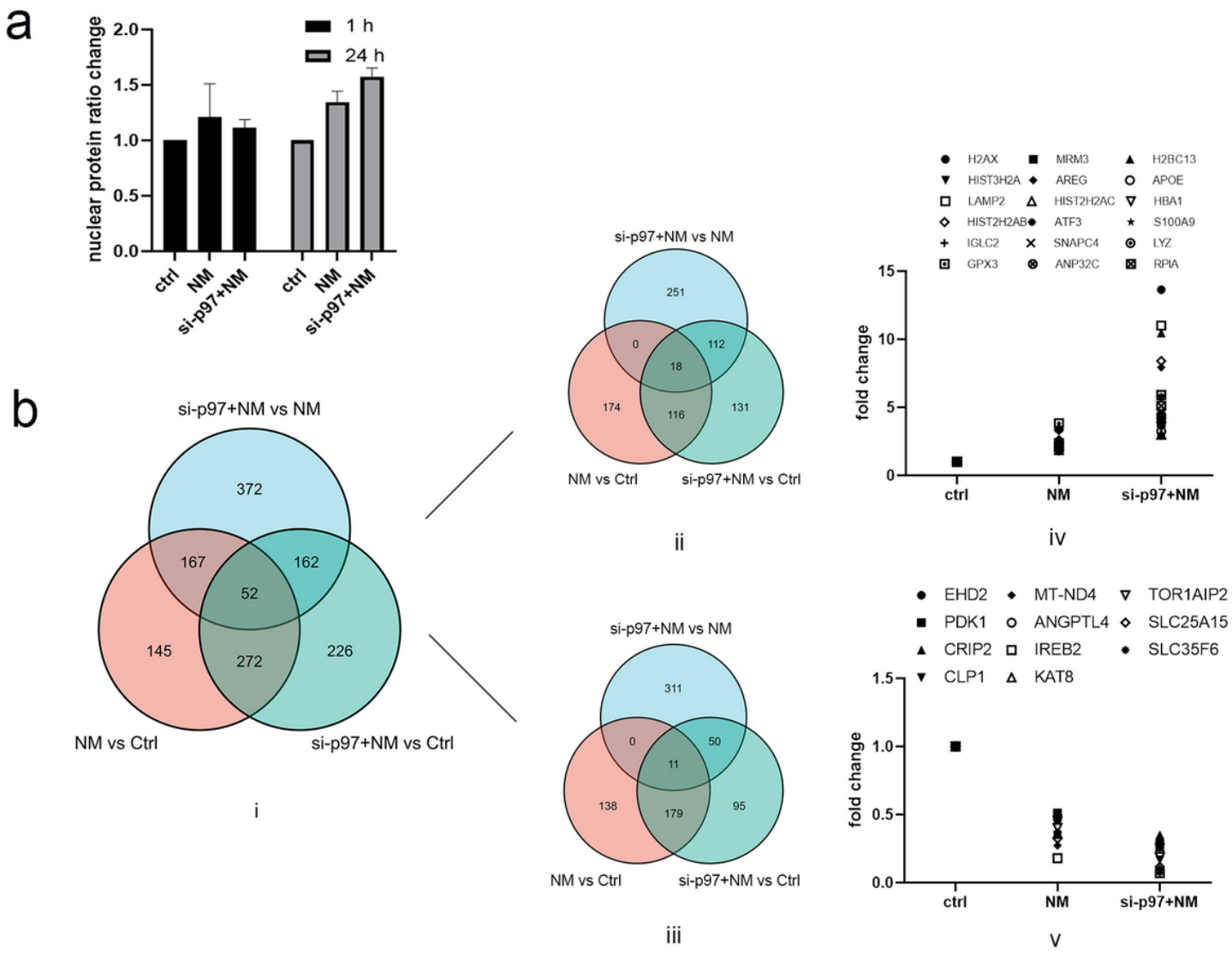

Figure 4

Overall changes of nuclear protein after 24 h of NM injury. (a) The ratio changes of the amount of nuclear protein to total protein in NM and NM+si-p97 groups at different time. Adjusted by setting the ratio of nuclear to total protein in control as 1. (b) i: After 24 h of NM treatment, the number of intra-nuclear differential proteins under the pairwise comparison of the three groups were classified by Venn diagram. ii-iii: The up-regulated and down-regulated proteins in the nucleus at 24 h were classified by Venn diagram. ii: up-regulated protein, iii: down-regulated protein. iv-v: the exact proteins and their fold changes in the middle part of Venn graph in ii and iii.

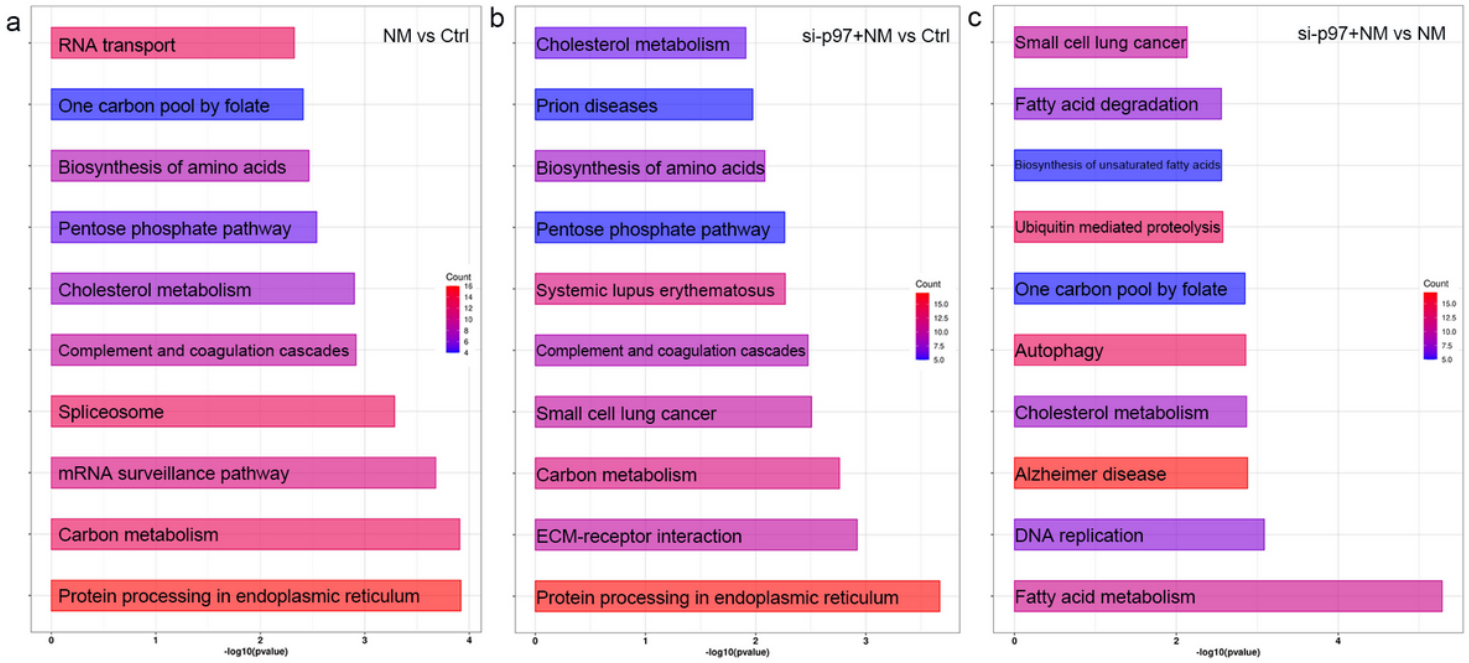

Figure 5

KEGG clustering of the differential proteins in the nucleus 24 h after NM injury. (a-c) After 24 h of NM treatment, the differential proteins of the three groups were compared in pairs and sequenced into the top ten pathways after KEGG clustering. The abscissa was -log10(p value), and the ordinate was the name of the pathway. Among them, the longer column indexed the smaller p-value, and the redder column indexed the more differentially expressed proteins in this pathway.

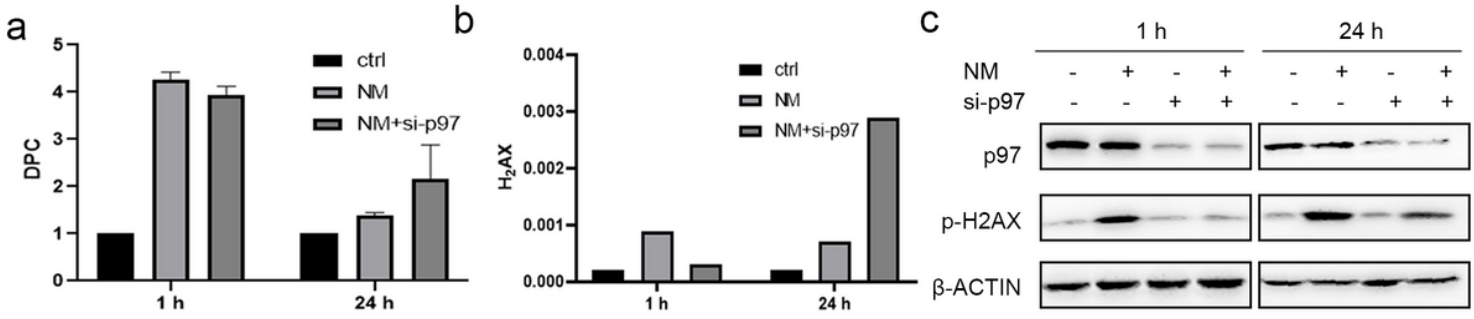

Figure 6

Effects of p97 on DNA damage induced by NM. (a) The effect of NM and si-p97 on DPC content at 1 h and 24 h. (b) The relative expression level of H2AX at 1 h and 24 h detected by Tandem Mass Tags spectrometry. (c) The effect of NM and si-p97 on p-H2AX content by WB detection.

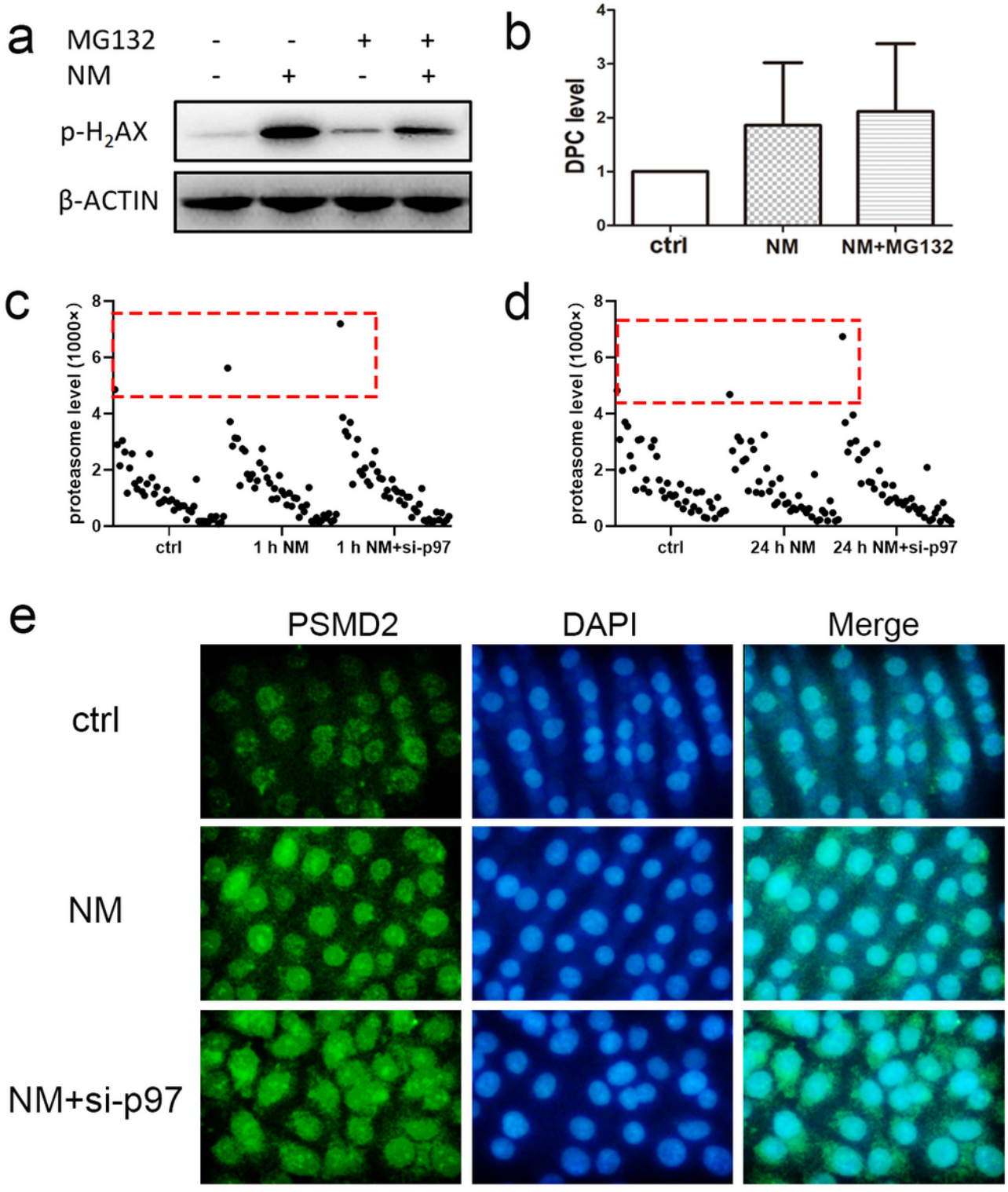

Figure 7

Effects of proteasome on NM-induced DNA damage. (a) The effect of NM and MG132 on the content of p-H2AX at 1 h by WB detection. (b) The effect of NM and MG132 on the DPC content at 24 h. (c, d) The relative expression level of all the subunits of proteasome at different treatment groups and time points. PSMD2 was Dots in the red dot line box. c: 1 h, d: 24 h. (e) Immunofluorescent staining of PSMD2.

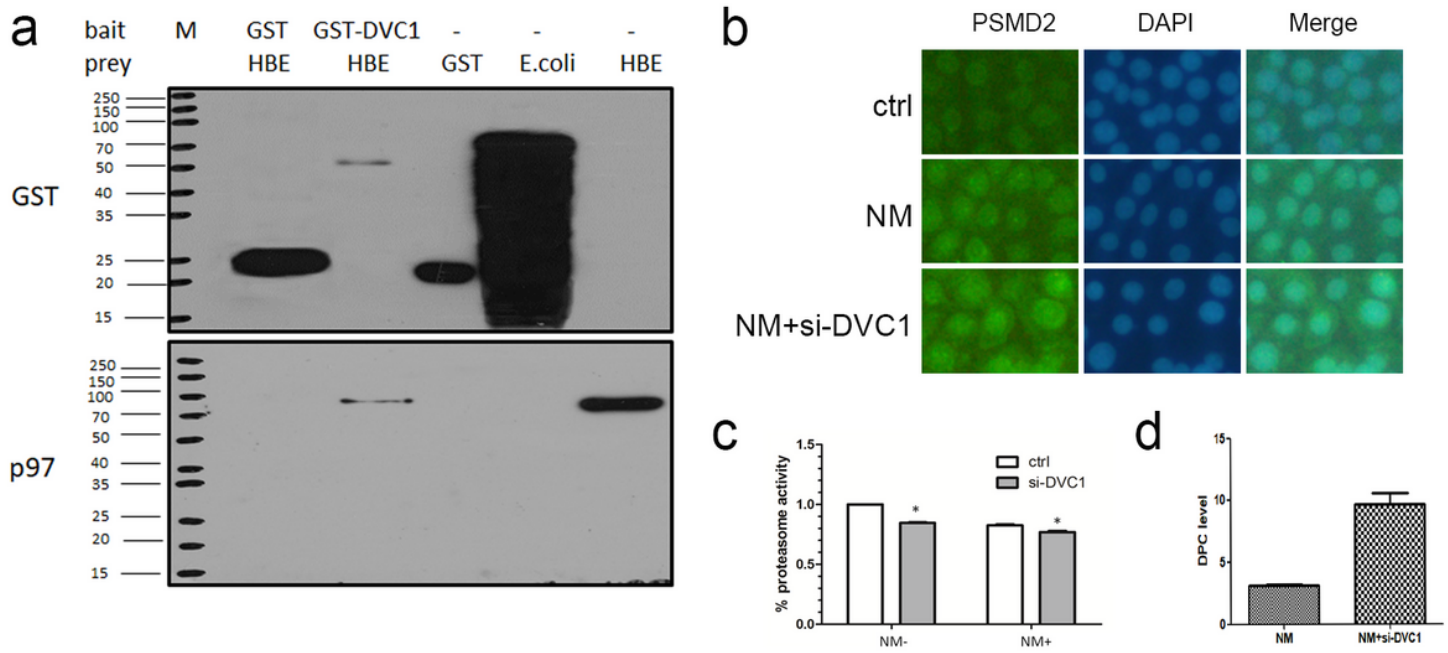

Figure 8

Role of DVC1 in the repair of NM-inducedDPC injury. (a) The interaction of DVC1 andp97. (b) The content and location of PSMD2 after NM or in combination with si-DVC1 treatment. (c) The effect of si-DVC1 on proteasome activity. *, *P*<0.05 vs ctrl. (d) The DPC level in si-DVC1 treatment.